AIP | Applied Physics Letters

Spin-orbit torques in Ta/TbxCo100-x ferrimagnetic alloy films with bulk perpendicular magnetic anisotropy

Kohei Ueda, Maxwell Mann, Chi-Feng Pai, Aik-Jun Tan, and Geoffrey S. D. Beach

Citation: Applied Physics Letters **109**, 232403 (2016); doi: 10.1063/1.4971393
View online: http://dx.doi.org/10.1063/1.4971393
View Table of Contents: http://scitation.aip.org/content/aip/journal/apl/109/23?ver=pdfcov
Published by the AIP Publishing

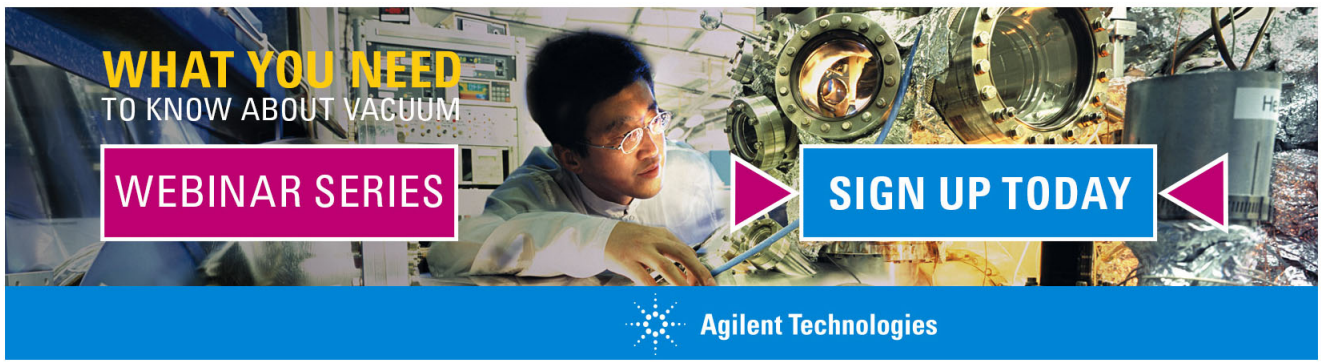

Spin-orbit torques in Ta/Tb_xCo_{100-x} ferrimagnetic alloy films with bulk perpendicular magnetic anisotropy

Kohei Ueda, Maxwell Mann, Chi-Feng Pai,[a] Aik-Jun Tan, and Geoffrey S. D. Beach[b]
Department of Materials Science and Engineering, Massachusetts Institute of Technology, Cambridge, Massachusetts 02139, USA

(Received 18 September 2016; accepted 21 November 2016; published online 5 December 2016)

We quantified the bulk perpendicular magnetic anisotropy (PMA) and spin-orbit torques (SOTs) in bilayer Ta/Tb_xCo_{100-x} ferrimagnetic alloy films with varying Tb concentration. The coercivity increases dramatically with increasing Tb_xCo_{100-x} thickness and is enhanced by the presence of a Ta underlayer. The Ta underlayer simultaneously serves as a source of SOT due to the spin Hall effect, which we show provides an efficient means to manipulate the magnetization in bulk PMA materials. It is further shown that the sign of the anomalous Hall voltage is different for rare-earth (RE) and transition-metal (TM) dominated alloy compositions, whereas the sign of the SOT effective field remains the same, suggesting that the former is related to the TM sublattice magnetization whereas the latter is related to the net magnetization. Our results suggest that Ta/Tb_xCo_{100-x} is a potential candidate for spin-orbitronic device applications and give insight into spin transport and SOTs in rare-earth/transition-metal alloys. *Published by AIP Publishing.*
[http://dx.doi.org/10.1063/1.4971393]

Spin-orbit torque (SOT) from the spin Hall effect (SHE)[1,2] has generated considerable interest for manipulating the magnetization in spintronic devices with ultra-low dissipation.[3–20] Recent research has demonstrated highly efficient magnetization switching[4–6] and magnetic domain wall (DW) motion[21–30] by current-induced SOT in ferromagnet (FM)/heavy metal (HM) bilayer films. In order to ensure scalability and thermal stability in device applications, the FM layer in such structures must exhibit perpendicular magnetic anisotropy (PMA). Thus far, most work on SOT in PMA films has focused on FM layers with interfacial PMA generated by adjacent HM or oxide layers. However, the interfacial anisotropy energy density in such films is insufficient to maintain thermal stability for bits scaled below ~20 nm.[31,32] Bulk PMA materials, such as L10-ordered alloys (FePt, FePd, CoPt, etc.),[32–35] Heusler alloys,[36,37] and rare earth-transition metal (RE-TM) alloys,[14,29–31,38–44] are potential candidates for devices since these materials provide a considerably larger volume anisotropy energy barrier. Furthermore, since the PMA of these materials is less sensitive to the nature of the interfaces, the adjacent layer materials can be optimized to maximize the SOTs without impacting the PMA. However, so far, there have been only a few studies of current-induced torques in bulk PMA materials, focusing mainly on current-induced domain wall motion by spin-transfer torques[33] or SOT.[29,30]

Ferrimagnetic RE-TM alloys are of particular interest because in addition to exhibiting bulk PMA, the saturation magnetization (M_s) is generally smaller than that in ferromagnetic metals due to partial compensation of the magnetization in opposing sublattices. Since the magnitude of SHE-induced SOTs scales inversely with M_s,[4,20] the switching efficiency in relatively thick ferromagnet/HM bilayer films might therefore be anticipated to be comparable to or even higher than in ultrathin FM/HM stacks, despite the larger anisotropy energy barrier that must be overcome in the former.

In this paper, we characterize SOTs in ferrimagnetic Tb_xCo_{100-x} alloy films generated by the SHE in a Ta underlayer. We examine two alloy compositions corresponding to both RE-dominant and TM-dominant net magnetizations, in order to determine the influence on spin transport and SOTs. We show that strong out-of-plane (OOP) anisotropy can be maintained for film thicknesses up to at least 16 nm, indicating a substantial bulk contribution to the PMA in these films. We then quantify the Slonczewski-like SOT in 8 nm thick Ta/Tb_xCo_{100-x} bilayers through current-induced hysteresis loop shift measurements.[19] Measurements show current-induced effective fields corresponding to an effective spin Hall angle of ~0.11 to 0.17, which compares well to prior results for Ta. Interestingly, we find that the sign of the anomalous Hall voltage is different for RE and TM dominated compositions, whereas the sign of the SOT effective field remains the same, suggesting that the former is related to the TM sublattice magnetization whereas the latter is related to the net magnetization.

We prepared Tb_xCo_{100-x} (TbCo) alloy films with Tb atomic percent $x = 21$ and $x = 33$ by dc co-sputtering from Tb and Co targets, with the alloy concentration determined from the calibrated sputtering rates. The depositions were performed at room temperature under 3.7 mTorr of Ar with a base pressure of 3×10^{-7} Torr, using thermally-oxidized Si substrates. The net magnetization of these two compositions is expected[40–42] to be Co dominated and Tb dominated, respectively, at room temperature.

We first examined two series of $Tb_{21}Co_{79}(t_{TbCo})$ films with varying TbCo thickness t_{TbCo}, both without and with a 3 nm thick dc sputtered Ta underlayer. All films were capped

[a]Present address: Department of Materials Science and Engineering, National Taiwan University, Taipei 10617, Taiwan.
[b]Author to whom correspondence should be addressed. Electronic mail: gbeach@mit.edu

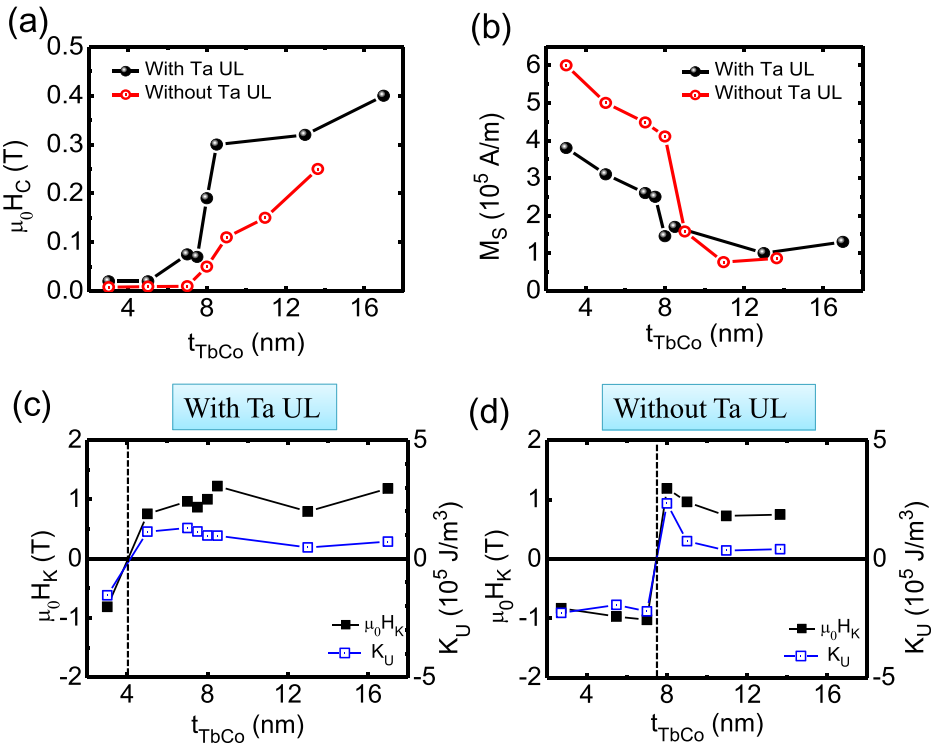

FIG. 1. (a) Coercive field (μ_0H_c) and (b) saturation magnetization (M_s) as a function of $Tb_{21}Co_{79}$ thickness (t_{TbCo}) with and without a Ta underlayer. (c) and (d) Magnetic anisotropy field (μ_0H_k) and magnetic anisotropy energy density (K_u) as a function of t_{TbCo} for Ta underlayer thickness $t_{Ta} = 3$ nm. (d) Corresponding result for $t_{Ta} = 0$ nm. Dotted lines indicate the threshold thickness for generating bulk perpendicular magnetic anisotropy.

with a Ta(3 nm) layer, which is expected to be largely oxidized under ambient conditions so that its contribution to current-induced SOTs is small. Magnetic properties were characterized with a vibrating sample magnetometer (VSM) in the out-of-plane (OOP) and in-plane (IP) configurations, as summarized in Fig. 1. Figures 1(a) and 1(b) show coercivity μ_0H_c and saturation magnetization M_s, respectively, as a function of t_{TbCo}. μ_0H_c increases monotonically with t_{TbCo} and is significantly enhanced by the Ta underlayer. M_s also depends on the presence of the underlayer and is larger for films grown directly on the thermally-oxidized substrate. Similar effects have been reported elsewhere[39] and attributed to preferential oxidation of the rare-earth metal by reduction of the substrate thermal oxide layer, which changes the surface roughness and alloy content. The anisotropy field μ_0H_k and effective magnetic anisotropy energy density $K_u = \mu_0M_sH_k/2$ with $H_k = H_{sat} + 4\pi M_s$ are plotted versus t_{TbCo} for the cases with a Ta underlayer (Fig. 1(c)) and without (Fig. 1(d)), where a positive sign indicates the out-of-plane anisotropy. Here, H_{sat} is the hard axis saturation field. Both H_k and K_u show a similar trend with t_{TbCo} for both series of samples. We find a threshold thickness (dotted lines in Figs. 1(c) and 1(d)) for generating PMA, suggesting that the film structure at low thicknesses is different from bulk. At larger thicknesses, the PMA energy density varies weakly with film thickness, consistent with a dominantly bulk contribution to the PMA. We find that the Ta underlayer promotes films with higher μ_0H_c and PMA at lower threshold thicknesses.

Next, we characterize the Slonczewski-like SOT generated by the SHE in the Ta underlayer, by means of current-assisted hysteresis loop shift measurements, following a technique developed earlier.[19] Out-of-plane (OOP) hysteresis loops are measured as a function of in-plane bias field for various injected currents I_{DC}. In this configuration, with the bias field along the current-flow direction, the Slonczewski-like effective field possesses an out-of-plane component $\mu_0H_z^{eff}$ that leads to a current-induced shift of the OOP hysteresis loop. Due to the limited field range for the out-of-plane magnet in our setup, we focus on thinner (8 nm) TbCo films to examine SOTs. We first studied $Tb_{21}Co_{79}$ films in which the Ta underlayer thickness t_{Ta} was varied from 4 to 8 nm in 2 nm increments to examine the effect of the SHE. Fig. 2(a) shows VSM OOP and IP hysteresis loops for $t_{Ta} = 6$ nm, indicating PMA with $\mu_0H_c = 0.1$ T. As shown in Fig. 2(b), μ_0H_c and M_s are relatively independent of t_{Ta} in this range.

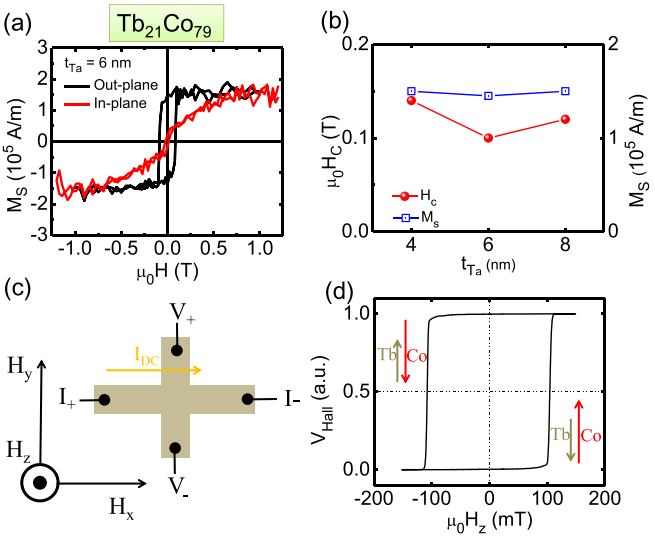

FIG. 2. (a) Vibrating sample magnetometer result with field applied in the out-of-plane and in-plane directions for $t_{Ta} = 6$ nm. (b) Coercive field (μ_0H_c) and saturation magnetization (M_s) as a function of t_{Ta}. (c) Illustration of device structure with measurement set-up. Directions of DC current flow (I_{DC}), out-of-plane applied field (μ_0H_z), longitudinal field along wire (μ_0H_x) and transverse field (μ_0H_y) are shown. (d) Hysteresis loop under μ_0H_z for $t_{Ta} = 6$ nm.

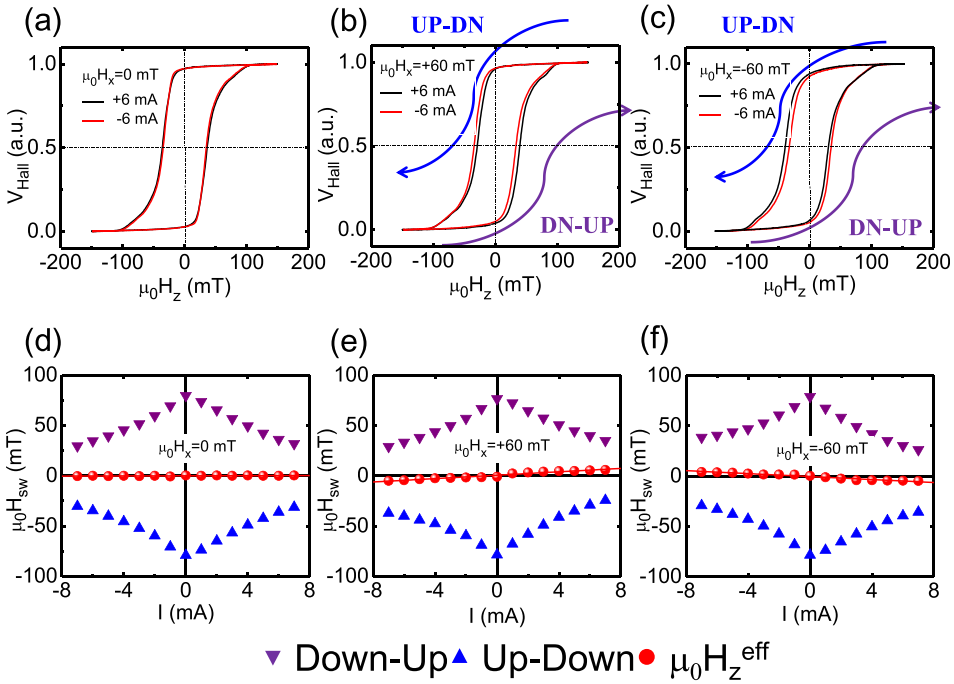

FIG. 3. (a)–(c) Typical out-of-plane hysteresis loops for (a) $\mu_0H_x = 0$ mT, (b) $\mu_0H_x = +60$ mT and (c) $\mu_0H_x = -60$ mT. (d)–(f) Switching field (μ_0H_{sw}) as a function of DC current flow for various (d) $\mu_0H_x = 0$ mT, (e) $\mu_0H_x = +60$ mT, and (f) $\mu_0H_x = -60$ mT. Red symbol and the fitting line show effective field ($\mu_0H_z^{eff}$) and spin-orbit torque efficiency.

To perform hysteresis loop shift measurements, we patterned 5 μm wide by 12 μm long Hall bars by photolithography and lift-off and used the anomalous Hall effect (AHE) to monitor the OOP magnetization electrically using a standard lock-in technique. Fig. 2(c) illustrates the measurement configuration. The DC current flows in the direction labeled I_{DC}. Applied fields are labeled H_z, H_x and H_y for OOP, longitudinal, and transverse to I_{DC}, respectively. Fig. 2(d) shows a typical AHE hysteresis loop under μ_0H_z for $t_{Ta} = 6$ nm.

Figures 3(a)–3(c) show AHE hysteresis loops for the same sample under I_{DC} without and with a longitudinal in-plane bias field of $\mu_0H_x = \pm 60$ mT. As can be seen, no current-induced loop shift occurs for $I_{DC} = 0$ mA, whereas a current-polarity-dependent loop shift is evident for $I_{DC} = \pm 6$ mA. The direction of the loop shift reverses when the direction of μ_0H_x reverses. These characteristics are consistent with the OOP effective field expected from the Slonczewski-like SOT. Figs. 3(d)–3(f) show the switching fields H_{SW} for up-to-down and down-to-up transitions, and the OOP loop centers as a function of I_{DC} for the indicated bias field conditions. The switching fields uniformly decrease with increasing $|I_{DC}|$, which is indicative of Joule-heating induced coercivity reduction. In addition, a shift of the loop center, proportional to I_{DC}, is observed for finite μ_0H_x, corresponding to the current-induced effective field $\mu_0H_z^{eff}$.

Figure 4(a) shows the slope of $\mu_0H_z^{eff}$ per unit current density flowing in the Ta layer, estimated from a parallel resistor model using the measured resistivities of individual Ta (370 $\mu\Omega$-cm) and $Tb_{21}Co_{79}$ (290 $\mu\Omega$-cm) layers. This slope, corresponding to the SOT efficiency χ, was measured as a function of longitudinal and transverse bias field. In the case of a transverse field, no loop shifts are observed and $\mu_0H_z^{eff} = 0$, as expected for Slonczewski-like torque. In the case of a longitudinal field, χ varies linearly with μ_0H_x and saturates above a threshold. We note that we observe neither a loop shift nor a change in coercivity under application of transverse fields up to at least 100 mT, indicating that the field-like torque, if present, has at most a very small influence on the measured switching fields.

This behavior has been previously observed and described in terms of domain nucleation and propagation during the reversal process.[19] Sweeping the OOP field nucleates reverse domains that expand across the film. For domain wall (DW) propagation-limited reversal, the effect of current can be understood through its effect on DW motion. Slonczewski-like SOT exerts an OOP effective field on DWs when the DW moment aligns along the current-flow direction. In the case of homochiral Néel DWs such as those that occur in PMA thin films with HM interfaces, the effective fields in the DWs on either side of a domain drive the DWs in the same direction rather than causing domain expansion or contraction. However, an in-plane bias field along the current-flow direction tends align DW moments in the same direction, so that the current-induced effective fields in the DWs at either end of a domain orient in the same direction and drive the domain to expand (contract), assisting (impeding) field-driven reversal. In this model,[19] the saturation of χ at large μ_0H_x thus corresponds to the threshold field to orient the DWs along the bias field direction, which depends on the DW shape anisotropy field (preferring Bloch DWs over Néel) and the Dzyaloshinskii-Moriya interaction (DMI)

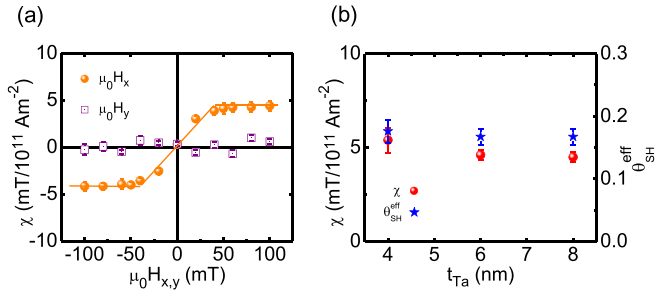

FIG. 4. (a) Spin-orbit-torque efficiency (χ) as a function of μ_0H_x and μ_0H_y. The line is a guide for the eye. (b) χ and spin Hall angle as a function of Ta under layer thickness.

strength (stabilizing homochiral Néel DWs). Above this threshold, the current-induced effective field is maximized and saturates at a value[19] $\mu_0 H_z^{\text{eff}} = \frac{\hbar \theta_{SH}^{eff}}{2eM_S t_{TbCo}} j$, where $\hbar$ is the Plank constant, θ_{SH}^{eff} is the effective spin Hall angle, e is the electron charge, and j is the current density. A transverse field $\mu_0 H_y$, by contrast, orients the DW moments orthogonal to the current flow such that the current-induced effective field is expected to vanish, consistent with our observation.

Figure 4(b) shows that the saturation SOT efficiency $\chi \approx |4.6 \pm 0.3|\,\text{mT}/(10^{11}\,\text{Am}^{-2})$ is independent of the Ta underlayer thickness for the range studied, which is to be expected for the SHE since t_{Ta} in this case exceeds the spin diffusion length of Ta, which is from ~1.4 nm[11] to 2.7 nm.[45] Using this saturation efficiency, we estimate θ_{SH}^{eff} through the relation[19] in the preceding paragraph to be $\sim 0.17 \pm 0.02$ (Fig. 4(b)). This value is consistent with the results of other reports for Ta,[4,19] indicating that the SHE in the Ta layer is likely responsible for the Slonczewski-like torque in this bulk-PMA film.

Next, we discuss the field at which χ saturates, as shown in Fig. 4(a). The saturation field is generally expected to occur when the DW moment fully aligns with the applied field, acting against the DW shape anisotropy field and the DMI, if present. We estimated the DW shape anisotropy field to be $\mu_0 H_{\text{DW}} \approx 70\,\text{mT}$ using the relation[27,46] $\mu_0 H_{DW} \approx \frac{M_s t \ln(2)}{\pi \Delta}$. Here, $\Delta = \sqrt{\frac{A}{K_u}}$ is the DW width, A is the exchange stiffness (1.0×10^{-12} J/m[47]) and t is the TbCo thickness. Since the estimated DW shape anisotropy field is close to the saturation field in Fig. 4(a), we conclude that the DMI is at most very weak in this system. We note that a recent study[44] of DW motion in thicker GdFeCo inferred the presence of homochiral DWs due to DMI arising from a composition and/or structural gradient, but we find no strong evidence for this effect in our experiments.

Finally, we examined a substrate/Ta(6 nm)/$Tb_{33}Co_{67}$(8 nm)/Ta(3 nm)-cap film with higher Tb content, in which the net magnetization is expected to be dominated by the RE sublattice.[38,40,41] Fig. 5(a) shows an AHE hysteresis loop under $\mu_0 H_z$. We find an inverted AHE voltage as compared to the $Tb_{21}Co_{79}$ film (Fig. 2(d)) in this case, where the Co sublattice is aligned antiparallel to the net magnetization. Since the sign of the anomalous Hall coefficient is the same (opposite) as in ferromagnetic Co PMA films,[46–48] for the Co-dominated (Tb-dominated) composition, we infer that the AHE reflects the magnetization of the TM sublattice rather than the net magnetization. These results are consistent with other reports on RE-TM alloys.[48–50]

Figures 5(b) and 5(c) show current-induced hysteresis loop shifts under in-plane bias fields for this sample. From these measurements, we determine χ versus $\mu_0 H_x$ and $\mu_0 H_y$, as plotted in Fig. 5(d). Similar to the Co-dominated film, we find no hysteresis loop shift for transverse fields and a linear increase in χ with $\mu_0 H_x$ up to a saturation value corresponding to $\theta_{SH}^{eff} \approx 0.11 \pm 0.02$. This value is somewhat smaller but reasonably consistent with θ_{SH}^{eff} obtained for the TM-dominated composition. The measured difference may reflect a difference in the spin-mixing conductance due to the different compositions. Notably, although the sign of the AHE is reversed for this composition, indicating a dominant

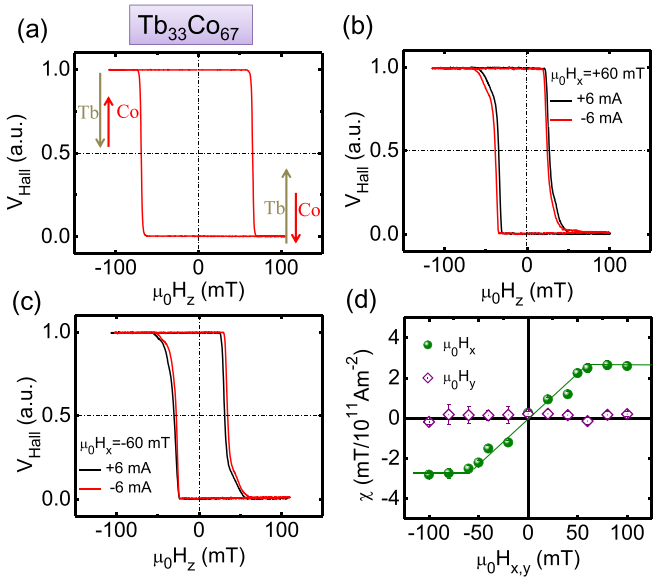

FIG. 5. (a) Hysteresis loop under $\mu_0 H_z$ in the absence of injected current and in-plane field. (b) and (c) Out-of-plane hysteresis loops with positive and negative dc bias currents I_{DC} for (b) $\mu_0 H_x = +60$ mT and (c) $\mu_0 H_x = -60$ mT. (d) χ as a function of $\mu_0 H_x$ and $\mu_0 H_y$. The line is a guide for the eye.

spin-transport interaction with the TM sublattice, the current-induced effective field is the same sign. Hence, we infer that the SHE-induced SOT is exerted on the net magnetization, rather than the Co sublattice. Finally, we note that a very recent study[51] in Ta/GdFeCo ferrimagnetic films also concluded that the AHE sign follows the TM sublattice magnetization, whereas the SOT acts on the net magnetization, consistent with our observations in Ta/TbCo.

In conclusion, we characterized the magnetic properties of co-sputtered Tb_xCo_{100-x} alloy films as a function of thickness, as well as the role of a Ta underlayer on these properties. We find that strong bulk PMA can be realized in films with thickness up to at least 16 nm and that the film properties are improved by a Ta underlayer. The Ta underlayer simultaneously provides a source for SOT via the SHE, generating a Slonczewski-like effective field corresponding to an effective spin Hall angle of ~0.11 to 0.17. Hence, SOTs can be used to efficiently manipulate the magnetization in relatively thick bulk anisotropy RE-TM films, with an efficiency similar to that in ultrathin FM/HM systems due to the relatively small M_s. Furthermore, we find that although the AHE reflects the magnetization of the TM sublattice, the SHE-induced torque tends to act on the net magnetization, giving further insight into spin transport and SOTs in rare-earth-containing materials. These results may help enable magnetic tunnel junction devices driven by SOT switching based on TM-RE alloy materials.

We thank Dr. F. Büttner and Dr. C. O. Avci for the fruitful discussion. This work was supported by the National Science Foundation under NSF-ECCS-1408172 and by the Samsung SGMI program.

[1]M. I. Dyakonov and V. I. Perel, Phys. Lett. A **35**, 459 (1971).
[2]J. E. Hirsch, Phys. Rev. Lett. **83**, 1834 (1999).
[3]M. Miron, K. Garello, G. Gaudin, P.-J. Zermatten, M. V. Costache, S. Auffret, S. Bandiera, B. Rodmacq, A. Schuhl, and P. Gambardella, Nature **476**, 189 (2011).

[4]L. Liu, C.-F. Pai, Y. Li, H. W. Tseng, D. C. Ralph, and R. A. Buhrman, Science **336**, 555 (2012).
[5]C.-F. Pai, L. Liu, Y. Li, H. W. Tseng, D. C. Ralph, and R. A. Buhrman, Appl. Phys. Lett. **101**, 122404 (2012).
[6]L. Liu, O. J. Lee, T. J. Gudmundsen, D. C. Ralph, and R. A. Buhrman, Phys. Rev. Lett. **109**, 096602 (2012).
[7]K. Garello, I. M. Miron, C. O. Avci, F. Freimuth, Y. Mokrousov, S. Blügel, S. Auffret, O. Boulle, G. Gaudin, and P. Gambardella, Nat. Nanotechnol. **8**, 587 (2013).
[8]J. Kim, J. Sinha, M. Hayashi, M. Yamanouchi, S. Fukami, T. Suzuki, S. Mitani, and H. Ohno, Nat. Mater. **12**, 240 (2013).
[9]S. Woo, M. Mann, A.-J. Tan, L. Caretta, and G. S. D. Beach, Appl. Phys. Lett. **105**, 212404 (2014).
[10]H.-R. Lee, K. Lee, J. Cho, Y.-H. Choi, C.-Y. You, M.-H. Jung, F. Bonell, Y. Shiota, S. Miwa, and Y. Suzuki, Sci. Rep. **4**, 6548 (2014).
[11]C. O. Avci, K. Garello, A. Ghosh, M. Gabureac, S. F. Alvarado, and P. Gambardella, Nat. Phys. **11**, 570 (2015).
[12]M. Akyol, J.-G. Alzate, G. Yu, P. Upadhyaya, K.-L. Wong, A. Ekicibil, P.-K. Amiri, and K.-L. Wang, Appl. Phys. Lett. **106**, 032406 (2015).
[13]C.-F. Pai, Y. Ou, L. H. Viela-Leao, D. C. Ralph, and R. A. Buhrman, Phys. Rev. B **92**, 064426 (2015).
[14]Z. Zhao, M. Jamali, A. K. Smith, and J.-P. Wang, Appl. Phys. Lett. **106**, 132404 (2015).
[15]K.-F. Huang, D.-S. Wang, H.-H. Lin, and C.-H. Lai, Appl. Phys. Lett. **107**, 232407 (2015).
[16]T. Nan, S. Emori, C.-T. Boone, X. Wang, T.-M. Oxholm, J.-G. Jones, B.-M. Howe, G.-J. Brown, and N.-X. Sun, Phys. Rev. B **91**, 214416 (2015).
[17]W. Zhang, W. Han, X. Jiang, S.-H. Yang, and S. S. P. Parkin, Nat. Phys. **11**, 496 (2015).
[18]K. Kondou, H. Sukegawa, S. Kasai, S. Mitani, Y. Niimi, and Y. Otani, Appl. Phys. Express **9**, 023002 (2016).
[19]C.-F. Pai, M. Mann, A. J. Tan, and G. S. D. Beach, Phys. Rev. B **93**, 144409 (2016).
[20]K. Ueda, C.-F. Pai, A. J. Tan, M. Mann, and G. S. D. Beach, Appl. Phys. Lett. **108**, 232405 (2016).
[21]I. M. Miron, T. Moore, H. Szambolics, L. D. Buda-Prejbeanu, S. Auffret, B. Rodmacq, S. Pizzini, J. Vogel, M. Bonfim, A. Schuhl, and G. Gaudin, Nat. Mater. **10**, 419 (2011).
[22]S. Emori, U. Bauer, S. M. Ahn, E. Martinez, and G. S. D. Beach, Nat. Mater. **12**, 611 (2013).
[23]K.-S. Ryu, L. Thomas, S.-H. Yang, and S. S. P. Parkin, Nat. Nanotechnol. **8**, 527 (2013).
[24]K.-S. Ryu, S.-H. Yang, L. Thomas, and S. S. P. Parkin, Nat. Commun. **5**, 3910 (2014).
[25]K. Ueda, K. J. Kim, Y. Yoshimura, R. Hiramatsu, T. Moriyama, D. Chiba, H. Tanigawa, T. Suzuki, E. Kariyada, and T. Ono, Appl. Phys. Express **7**, 053006 (2014).
[26]J. Torrejon, J. Kim, J. Sinha, S. Mitani, M. Hayashi, M. Yamanouchi, and H. Ohno, Nat. Commun. **5**, 4655 (2014).
[27]S. Emori, E. Martinez, K.-J. Lee, H.-W. Lee, U. Bauer, S.-M. Ahn, P. Agrawal, D. C. Bono, and G. S. D. Beach, Phys. Rev. B **90**, 184427 (2014).
[28]K. Ueda, K.-J. Kim, T. Taniguchi, T. Tono, T. Moriyama, and T. Ono, Phys. Rev. B **91**, 060405(R) (2015).
[29]D. Bang and H. Awano, J. Appl. Phys.**117**, 17D916 (2015).
[30]D. Bang, J. Yu, X. Qiu, Y. Wang, H. Awano, A. Manchon, and H. Yang, Phys. Rev. B **93**, 174424 (2016).
[31]N. Nishimura, T. Hirai, A. Koganei, T. Ikeda, K. Okano, Y. Sekiguchi, and Y. Osada, J. Appl. Phys. **91**, 5246 (2002).
[32]H. Wang, M. T. Rahman, H. Zhao, Y. Isowaki, Y. Kamata, A. Kikitsu, and J.-P. Wang, J. Appl. Phys. **109**, 07B754 (2011).
[33]P. He, L. Ma, Z. Shi, G. Y. Guo, J.-G. Zheng, Y. Xin, and S. M. Zhou, Phys. Rev. Lett. **109**, 066402 (2012).
[34]A. Itabashi, M. Ohtake, S. Ouchi, F. Kirino, and M. Futamoto, EPJ Web Conf. **40**, 07001 (2013).
[35]C. Burrowes, A. P. Mihai, D. Ravelosona, J.-V. Kim, C. Chappert, L. Vila, A. Marty, Y. Samson, F. Garcia-Sanchez, L. D. Buda-Prejbeanu, I. Tudosa, E. E. Fullerton, and J.-P. Attane, Nat. Phys. **6**, 17 (2010).
[36]S. Ouardi, T. Kubota, G. H. Fecher, R. Stinshoff, S. Mizukami, T. Miyazaki, E. Ikenaga, and C. Felser, Appl. Phys. Lett. **101**, 242406 (2012).
[37]H. Kurt, K. Rode, M. Venkatesan, P. Stamenov, and J. M. D. Coey, Phys. Rev. B **83**, 020405 (2011).
[38]P. Hansen, C. Clausen, G. Much, M. Rosenkranz, and K. J. Witter, Appl. Phys. **66**, 756 (1989).
[39]S. Q. Yin, X. Q. Li, X. G. Xu, J. Miao, and Y. Jiang, IEEE Trans. Magn. **47**, 3129 (2011).
[40]S. Alebrand, M. Gottwald, M. Hehn, D. Steil, M. Cinchetti, D. Lacour, E. E. Fullerton, M. Aeschlimann, and S. Mangin, Appl. Phys. Lett. **101**, 162408 (2012).
[41]S. Alebrand, U. Bierbrauer, M. Hehn, M. Gottwald, O. Schmitt, D. Steil, E. E. Fullerton, S. Mangin, M. Cinchetti, and M. A. Aeschlimann, Phys. Rev. B **89**, 144404 (2014).
[42]R. Tolley, T. Liu, Y. Xu, S. Le Gall, M. Gottwald, T. Hauet, M. Hehn, F. Montaigne, E. E. Fullerton, and S. Mangin, Appl. Phys. Lett. **106**, 242403 (2015).
[43]M. H. Tang, Z. Zhang, S. Y. Tian, J. Wang, B. Ma, and Q. Y. Jin, Sci. Rep. **5**, 10863 (2015).
[44]T. Tono, T. Taniguchi, K.-J. Kim, T. Moriyama, A. Tsukamoto, and T. Ono, Appl. Phys. Express **8**, 073001 (2015).
[45]M. Morota, Y. Niimi, K. Ohnishi, D. H. Wei, T. Tanaka, H. Kontani, T. Kimura, and Y. Otani, Phys. Rev. B **83**, 174405 (2011).
[46]S. V. Tarasenko, A. Stankiewicz, V. V. Tarasenko, and J. Ferré, J. Magn. Magn. Mater. **189**, 19 (1998).
[47]M. T. Rahman, X. Liu, M. Matsumoto, and A. Morisako, IEEE Trans. Magn. **41**, 2568 (2005).
[48]R. Asomoza, I. A. Campbell, H. Jouve, and R. Meyer, J. Appl. Phys. **48**, 3829 (1977).
[49]R. Malmhäll, J. Appl. Phys. **54**, 5128 (1983).
[50]S. Honda, M. Nawate, M. Ohkoshi, and T. Kusuda, J. Appl. Phys. **57**, 3204 (1985).
[51]N. Roschewsky, T. Matsumura, S. Cheema, F. Hellman, T. Kato, S. Iwata, and S. Salahuddin, Appl. Phys. Lett. **109**, 112403 (2016).